Integrated Guidance and Control for Homing Missiles

Neil F. Palumbo, Brian E. Reardon, and Ross A. Blauwkamp

The need to engage and negate highly maneuverable threats imposes stringent performance requirements on missile interceptors. The design challenges are significant and require advances in interceptor airframe, sensor and propulsion systems, and guidance and control (G&C) algorithms. In essence, the G&C algorithms must orchestrate the various interceptor components to maximize lethality across the threat space. To this end, traditional G&C designs use a *decoupled* architecture involving three discrete algorithms. Separate designs and weak functional interactions among the algorithms make interceptor performance optimization difficult. In this article, we introduce an alternate G&C architecture wherein the traditional elements are replaced by a single component that performs all three functions. This *integrated* G&C (IGC) paradigm facilitates a level of synergism between flight control and guidance functions that is difficult to emulate within a decoupled framework. Moreover, the IGC design process unifies interceptor performance optimization versus the decoupled approach. Using a six-degree-of-freedom simulation tool, we compare a prototype IGC algorithm to a benchmark G&C system using a decoupled structure. We show that the IGC concept significantly improves the mean and standard deviation of the final miss distance against stressing threats.

INTRODUCTION

Modern missile interceptors must engage and negate a variety of threats, including tactical ballistic missiles (TBMs) and high-performance cruise missiles. The need to engage such diverse and ever-evolving threats poses a significant challenge to interceptor design. For example, TBMs can have high velocity and, upon reentry, can exhibit complex coning motion and slowdown as they move through the atmosphere. Likewise, high-performance cruise missiles can fly at supersonic speeds, have high lateral acceleration capability, and can execute maneuvers that are difficult to anticipate. Given the types of payloads these threats can deliver, the missile interceptor design must ensure a high probability of payload kill (P_k) across a diverse threat space, despite the engagement stressors. What is more, the interceptor design must sufficiently outpace the projected capabilities and characteristics of both evolving and new threat missiles. Hence, next-generation interceptors will inevitably be required to fly faster, longer, and with more efficiency; see farther and with better resolution; and effectively outmaneuver the threat such that the required lethality is achieved.

Qualitatively, the aggregate capability of the interceptor subsystems will define a maximum performance potential. For a given interceptor configuration, the central role of the guidance and control (G&C) algorithms is to functionally integrate the subsystems to ensure that all requirements are met and that lethality is consistently maximized. To do this, several critical G&C functions must be considered. First, the missile must maintain stable flight and converge on the target such that the final distance between the interceptor and threat (final miss distance) is minimized. Pointing to allow seeker (onboard target sensor) acquisition and tracking is also a critical function. Another important task is to manage the interceptor energy to maximize range or time-of-flight capability. Often, the direction of approach must be controlled as well to maximize P_k. Clearly, the G&C algorithms must perform a variety of complex functions. In this light, neglecting the role that G&C plays in maximizing interceptor capability will lead to suboptimal performance and, possibly, higher-cost hardware to achieve a required level of performance.

Typically, guided missile flight is partitioned into three phases: boost, midcourse, and terminal. The complexity and criticality of each phase depends on the mission for which the interceptor was designed. Furthermore, not all guided missiles use all three phases.[1] However, all precision guided missiles have a terminal phase, which is the last and generally most critical phase.

Depending on the interceptor and mission, the terminal phase can begin anywhere from tens of seconds down to a few seconds before intercept. The purpose of the terminal phase is to remove the residual errors accumulated during the prior phases and ultimately to reduce the final distance between the interceptor and threat below some specified level. For systems that use a fuze and fragmentation warhead, this final miss distance must be less than the warhead lethal radius. In this case, the warhead lethal radius accommodates some lack of precision. On the other hand, a direct-hit missile can only tolerate very small "misses" relative to a selected aimpoint before compromising lethality. In either case, it is during this terminal phase of flight that the interceptor must have a high degree of accuracy and a quick reaction capability. Moreover, near the very end of the terminal phase (often referred to as the endgame), the interceptor may be required to maneuver to maximum capability in order to converge on and hit a fast-moving, evasive target. In this article, we focus on the terminal phase of flight with an emphasis on consistently minimizing the final miss distance.

Traditional Guidance and Control Architecture

The G&C system must functionally integrate the interceptor subsystems to ensure that all requirements are met and that lethality is consistently maximized across the range of threats of interest. Traditional G&C paradigms address this using a *decoupled* architecture comprising a guidance filter, guidance law, and autopilot. This decoupled structure is notionally illustrated in Fig. 1.

As indicated in the figure, the traditional architecture separates guidance and flight control functions. The guidance filter takes noisy target measurement data and estimates the relevant target states, the selection of which is design dependent.[2] For example, a Cartesian guidance filter can provide estimates of target position, velocity, and acceleration with respect to a Cartesian reference frame. Equivalently, relative (threat-interceptor) position, relative velocity, and target acceleration can be estimated. In general, a Kalman filter or an extended Kalman filter is used.[3] The guidance law takes the instantaneous target state estimates as input and determines what the interceptor direction of travel should be to intercept the threat. One of the oldest and most frequently used guidance laws is proportional navigation,[1,4,5] which generates guidance commands proportional to the line-of-sight rate between the guided missile and target. The autopilot is responsible for stabilization and command following.[1,6,7] It receives the guidance commands and issues the relevant aerodynamic (e.g., fin), thrust-vector, or divert control commands necessary to achieve the commanded acceleration. The inertial navigation system determines the instantaneous missile position and the direction in which it is currently heading. We focus here on the guidance filter, guidance law, and autopilot functions.

Certain attributes of the decoupled approach are worth noting. First, it is typical to design each component separately and, as suggested by Fig. 1, a variety of synthesis techniques may be adopted for each component design (only the dominant techniques are indicated). In some sense, this implies an unstructured approach to

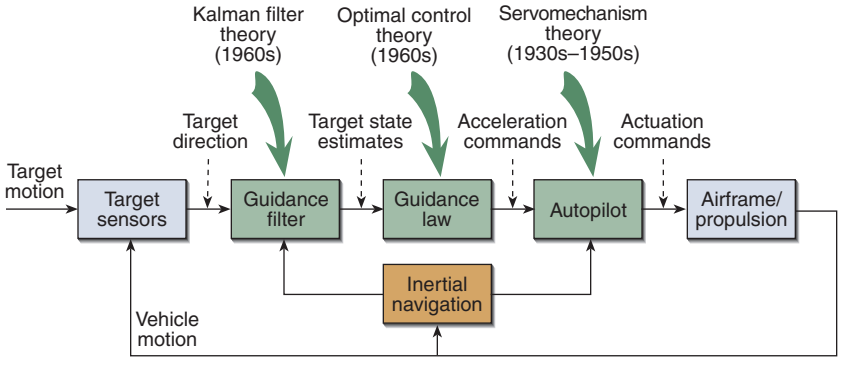

Figure 1. Traditional guidance and control designs use a decoupled architecture containing guidance filter, guidance law, and autopilot components.

interceptor performance optimization. Differing synthesis techniques for each component add to the unstructured nature of the decoupled design approach. Second, it is fair to say that little *a priori* consideration is made of desirable G&C component functional interaction (synergism) during the design process. Instead, simplifying assumptions are made to achieve an implementable solution. As a result, the system as a whole is iteratively tuned, adjusted, and/or modified until satisfactory performance is achieved. This usually leads to an overly conservative design. Hence, one can surmise that over the last 20 to 30 years, interceptor performance improvement has been realized largely by improving the interceptor subsystems (e.g., changing the missile airframe, improving the terminal sensor, adding side thrusters, etc.). Subsequently, existing (or incrementally evolved) G&C architectures and algorithms are used to integrate and control the advanced interceptor hardware. Instead, we suggest that innovative G&C architectures, coupled with modern synthesis techniques, can facilitate an optimal integration of the missile subsystems, thereby leading to a consistently high P_k across the threat space.

Integrated Guidance and Control Architecture

Exploiting the synergistic coupling that exists between the guidance (i.e., the information and prediction aspect of the problem) and flight control functions helps to achieve optimal interceptor performance. In contrast to the *decoupled* approach, a tightly *integrated* G&C (IGC) paradigm facilitates G&C synergism in addition to offering a structured approach to performance optimization. Figure 2 illustrates a notional IGC architecture. Note that G&C component separation has less meaning in an IGC design, that is, information and control are inseparable.

Synergistic Coupling and IGC

Many interceptor subsystems have interactions that can be exploited to optimize performance. For instance, at the G&C component level, an inverse relationship exists between information and prediction quality (i.e., guidance system accuracy) versus the necessary bandwidth of the flight control system to render a kill. An IGC system can explicitly accommodate this relationship. In part, this is due to the explicit knowledge of the airframe-plus-autopilot response that is available to the "guidance portion" of a fully integrated system. This is an important factor when, for example, one considers the generation of "optimal" guidance commands for tail-controlled (i.e., non-minimum phase) airframes.[8] In contrast, traditional guidance policies rely on simplifying assumptions regarding the acceleration response characteristics (e.g., first-order lag response) of missile interceptors.[4]

Figure 3 illustrates a typical (normalized) tail-controlled missile acceleration response to a unit-step acceleration input. The non-minimum phase characteristic is circled in the figure. Also shown is the acceleration response assumption typically made in a traditional guidance policy. Note that as the homing time falls within the missile time constant (the time it takes the response to achieve 63% of the command), the conventional guidance policy will issue acceleration commands in a direction opposite to what is needed. In contrast, an IGC approach predicts the missile response more accurately, thus providing significantly improved endgame performance: an IGC system generates guidance commands that account for the non-minimum phase acceleration response characteristic typical of tail-controlled missiles. This is crucial for endo-atmospheric interceptors requiring a high P_k.

Structured (Unified) Approach to Performance Optimization

Referring again to Fig. 2, a dynamic game, or *minimax*, formulation is used to synthesize the IGC system.

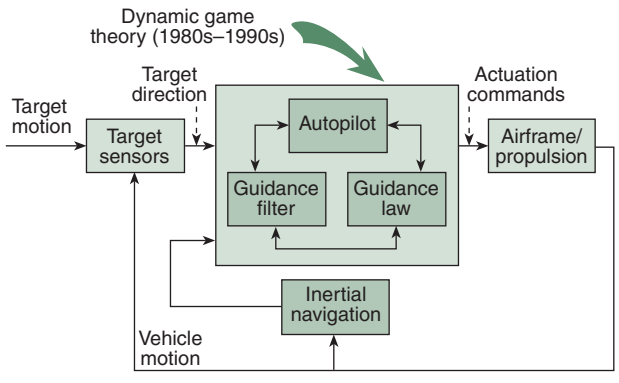

Figure 2. With an integrated guidance and control system, there is no separation of the guidance and flight control functions.

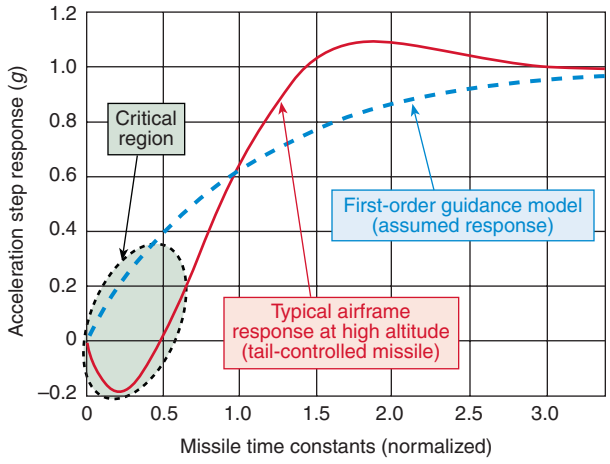

Figure 3. Non-minimum phase response to a unit-step acceleration command versus the "assumed" response of a traditional guidance model. Traditional guidance system models describe the interceptor acceleration response as a first-order lag. For tail-controlled missiles, this assumption can deviate significantly from the actual missile response.

Dynamic game theory is a superset of standard optimal control theory.[9–11] Formulating the design problem in this way adds an additional level of integration between the information and control functions that is not realized in conventional systems. The well-known result is that the control solution is a function of information uncertainty.[9,11] The implication is twofold: (1) the estimation and control functions are optimized together, and (2) the synergy between information quality and control action is better exploited, unlike in the decoupled designs. Thus, the optimization criterion can *explicitly* focus on larger objectives such as maximizing P_k. In fact, in an IGC system, one can explicitly specify and account for critical engagement parameters like final miss distance *and* endgame approach angle to maximize interceptor lethality. On the contrary, conventional guidance systems are adjusted in an *ad hoc* way to indirectly improve lethality.

Scope

The idea of integrating the G&C functions in a homing missile is not new. A number of papers have addressed the IGC concept over the past 20 years, with differing assumptions and varying levels of fidelity.[11–17] Our goal is to address the IGC problem to sufficient detail such that it can be applied to a tactical system design.

To synthesize a feedback control law, a mathematical model of the process to be controlled (the plant) is first defined. Our model is nonlinear and contains a combination of homing-loop kinematic (guidance) and missile body-motion states. We formulate the IGC problem as a finite-time-horizon dynamic game using partial-state information (measurement feedback).[9] The prototype IGC *minimax* design objective is to find a controller that minimizes the final miss distance and interceptor control energy under worst-case process and measurement disturbances. (Target maneuver and target sensor errors are examples of process and measurement disturbances, respectively.)

Because of the nonlinear nature of the problem, we use an approximation technique known as the state-dependent Riccati differential (difference) equation (SDRDE) method to obtain a solution.[18,19] This is a generalization of the state-dependent (algebraic) Riccati equation (SDRE) method first described in Ref. 20 and later in Refs. 11–13, 16, and 21. However, because published theoretical results or empirical data to support the SDRDE approach are scarce, many unanswered questions as to feasibility and applicability remain. We have found that, from a strictly performance-driven perspective, the SDRDE methodology is a viable solution technique for this class of problems, but this approach is computationally intensive. Moreover, the SDRDE technique requires a state-factorable representation of the plant dynamics. We address this by using a missile aerodynamic database during operation. (This database is constructed through wind tunnel experiments and is no different from that used for conventional G&C designs; i.e., the need to develop this database is not driven by the IGC design.) During operation, the database is interrogated at each sample-instant to estimate the missile forces and moments, and an appropriate state factorization is performed. This technique is general in nature and has performed well in simulation with two different high-fidelity nonlinear aerodynamics models.

We begin the subsequent discussion by focusing on the modeling and control-theoretic aspects of designing an IGC system. First we set up the problem, state the relevant assumptions, and summarize the theoretical solution framework we employ. Next, we summarize the modeling aspects of an IGC problem. Together, these discussions illustrate the structure of the IGC solution and are included for completeness. A cursory reading will give the reader enough background to move on through the article. As within any control problem, there are "tuning knobs" within the IGC solution structure that must be adjusted to provide optimum performance. Thus, we continue this article by discussing simulation-based performance optimization (that is, using the computer to iteratively seek the best tuning) and present simulation results showing IGC system performance versus a benchmark G&C system.

THE IGC SOLUTION FRAMEWORK

The IGC plant model can be expressed by the following nonlinear input-affine continuous-time equations:

$$\begin{aligned} \dot{\mathbf{x}}(t) &= \mathbf{f}(\mathbf{x}, t) + \mathbf{b}(\mathbf{x}, t)\mathbf{u}(t) + \mathbf{D}(\mathbf{x}, t)\mathbf{w}(t), \mathbf{x}(0) = \mathbf{x}_0 \\ \mathbf{y}(t) &= \mathbf{c}(\mathbf{x}, t) + \mathbf{E}(\mathbf{x}, t)\mathbf{w}(t) \\ z(t) &= \mathbf{h}(\mathbf{x}, t) + \mathbf{g}(\mathbf{x}, t)\mathbf{u}(t)\,. \end{aligned} \tag{1}$$

The first part of Eq. 1 describes a nonlinear plant with state vector $\mathbf{x}(t) \in \mathbb{R}^n$, driven by control input vector $\mathbf{u}(t) \in \mathbb{R}^m$ and subject to a set of exogenous input variables represented by vector $\mathbf{w}(t) \in \mathbb{R}^r$, which includes disturbances to be rejected and possibly references to be tracked. The second part of the equation defines a set of measured variables represented by vector $\mathbf{y}(t) \in \mathbb{R}^p$, which are functions of the state vector $\mathbf{x}(t)$ and exogenous input vector $\mathbf{w}(t)$. The third part of the equation defines a performance output vector $z(t) \in \mathbb{R}^s$. The designer specifies the performance output vector to be those components of the state and control vectors deemed crucial to the design problem. Above, $\mathbf{f}(\mathbf{x}, t)$, $\mathbf{b}(\mathbf{x}, t)$, $\mathbf{c}(\mathbf{x}, t)$, $\mathbf{h}(\mathbf{x}, t)$, and $\mathbf{g}(\mathbf{x}, t)$ are nonlinear vector functions and $\mathbf{D}(\mathbf{x}, t)$ and $\mathbf{E}(\mathbf{x}, t)$ are matrices of appropriate dimensions. It is assumed that all the functions are smooth and that $\mathbf{f}(\mathbf{x} = 0, t) = 0$, $\mathbf{c}(\mathbf{x} = 0, t) = 0$, and finally that $\mathbf{b}(\mathbf{x}, t) \neq 0 \forall \mathbf{x}$ holds for every t.

Extended Linearization

As is characteristic in aerospace applications, the IGC plant model is nonlinear. Typically, this issue is addressed within a linear design framework using a gain scheduling approach.[22] One first develops a set of linearized plant models at a large number of flight conditions and designs a control law for each linearized model using an appropriate synthesis technique. The control law parameters (gains) are scheduled during flight as functions of dynamic pressure and possibly altitude, Mach, time of flight, etc. We have adopted an alternate approach to controller design based on the *extended linearization* concept.[11,13,20,21] Extended linearization is the process of factoring a nonlinear system such that it has a "linear-looking" structure with plant matrices that are *state-dependent*. Then, any number of synthesis techniques may be applied. For example, consider how the following nonlinear plant is parameterized to derive a linear-looking but state-dependent structure:

$$\begin{pmatrix}\dot{x}_1\\ \dot{x}_2\end{pmatrix}=\begin{pmatrix}x_1-x_1^3+x_2+u_1\\ x_1+x_1^2x_2-x_2+u_2\end{pmatrix}\underset{\text{Parameterize}}{\Rightarrow}\begin{pmatrix}\dot{x}_1\\ \dot{x}_2\end{pmatrix}=\begin{pmatrix}1-x_1^2 & 1\\ 1 & x_1^2-1\end{pmatrix}\begin{pmatrix}x_1\\ x_2\end{pmatrix}+\begin{pmatrix}1 & 0\\ 0 & 1\end{pmatrix}\begin{pmatrix}u_1\\ u_2\end{pmatrix}. \tag{2}$$

This example illustrates one of an infinite number of possible parameterizations that can be applied to bring the nonlinear plant to state-dependent form.

We can bring Eq. 1 to a state-dependent form. Applying a linear control synthesis technique to such a system suggests that the control solution is recomputed periodically in the flight computer. Therefore, we will implement a discrete-time control solution. At each sample-instant, the continuous-time (state-dependent) system is discretized[23] as indicated below.

$$\begin{aligned}\dot{\mathbf{x}}(t)&=\mathbf{A}(\mathbf{x},t)\mathbf{x}(t)+\mathbf{B}(\mathbf{x},t)\mathbf{u}(t)+\mathbf{D}(\mathbf{x},t)\mathbf{w}(t)\\ \mathbf{y}(t)&=\mathbf{C}(\mathbf{x},t)\mathbf{x}(t)+\mathbf{E}(\mathbf{x},t)\mathbf{w}(t)\\ \mathbf{z}(t)&=\mathbf{H}(\mathbf{x},t)\mathbf{x}(t)+\mathbf{G}(\mathbf{x},t)\mathbf{u}(t)\end{aligned}\quad\underset{\text{Discretize}}{\Rightarrow}\quad\begin{aligned}\mathbf{x}_{k+1}&=\mathbf{A}_k\mathbf{x}_k+\mathbf{B}_k\mathbf{u}_k+\mathbf{D}_k\mathbf{w}_k\\ \mathbf{y}_k&=\mathbf{C}_k\mathbf{x}_k+\mathbf{E}_k\mathbf{w}_k\\ \mathbf{z}_k&=\mathbf{H}_k\mathbf{x}_k+\mathbf{G}_k\mathbf{u}_k\end{aligned} \tag{3}$$

Here, $\mathbf{A}(\mathbf{x}, t)$, $\mathbf{B}(\mathbf{x}, t)$, $\mathbf{C}(\mathbf{x}, t)$, $\mathbf{D}(\mathbf{x}, t)$, $\mathbf{E}(\mathbf{x}, t)$, $\mathbf{H}(\mathbf{x}, t)$, and $\mathbf{G}(\mathbf{x}, t)$ are state-dependent matrices of compatible dimensions, and k represents discrete time. Above, the relationship of the discrete-time elements to continuous-time counterparts is straightforward. Note that state dependence in the discrete-time system is implied but not explicitly shown. We will discuss state factorization for our problem in more detail below.

Linear-Quadratic Dynamic Game Formulation

For the moment, we ignore the fact that the plant matrices are state-dependent. The IGC problem is posed as a dynamic game with partial state information (PSI); that is, we consider a measurement feedback structure of the form $\mathbf{u}_k=\mathbf{U}(\{\mathbf{y}_l\}_{l=0}^{k})$, where k represents the current discrete time. In a dynamic game, the system disturbances, rather than being modeled as white noise, are modeled as an *opposing player* whose strategy is to maximize the control actions necessary to achieve intercept. The control $\mathbf{u}_k$ must counter these worst-case disturbances. The control objective is to keep a function of the performance output $\mathbf{z}_k$ and terminal state $\mathbf{x}_N$ (state vector at the final time) small, despite unpredictable disturbances $\mathbf{w}_k$ and initial estimation errors $\mathbf{x}_0-\hat{\mathbf{x}}_0$. This is accomplished by solving the following discrete-time, soft-constrained dynamic game, subject to Eq. 3 (Ref. 9):

$$\min_{\mathbf{u}_k}\max_{\mathbf{w}_k}J_\gamma(\mathbf{u}_k,\mathbf{w}_k)=\left|\mathbf{x}_N\right|_{\mathbf{Q}_f}^2-\gamma^2\left|\mathbf{x}_0-\hat{\mathbf{x}}_0\right|_{\mathbf{Q}_0}^2+\sum_0^{N-1}\left\{\left|\mathbf{z}_k\right|^2-\gamma^2\left|\mathbf{w}_k\right|^2\right\}. \tag{4}$$

In Eq. 4, known as the performance index of the game, $|.|_{\mathbf{M}}$ represents a Euclidian norm weighted by matrix $\mathbf{M}$, $\hat{\mathbf{x}}_0$ is the initial state-vector estimate, and N is the time over which the optimization is carried out. The desired disturbance attenuation level γ is a bound on the worst-case amplification of the disturbances to the performance index by the controlled system. This must satisfy $\gamma\geq\gamma^*$, where γ^* denotes the limiting achievable disturbance attenuation performance level.

Recall that the role of the disturbance $\mathbf{w}_k$ is to maximize the performance index. As $\gamma\to\infty$, the game converges to the standard, disturbance-free, optimal control problem with quadratic cost. The initial estimation error and terminal penalty weighting matrices $\mathbf{Q}_0$ and $\mathbf{Q}_f$ are assumed to be positive definite, $\mathbf{Q}_0$, $\mathbf{Q}_f>0$. Also, the following point-wise conditions are assumed to hold: $\mathbf{G}_k^T\mathbf{G}_k\equiv\mathbf{R}_k>0$, $\mathbf{H}_k^T\mathbf{H}_k\equiv\mathbf{Q}_k\geq 0$, $\mathbf{E}_k\mathbf{E}_k^T\equiv\mathbf{N}_k>0$,

rank $[\mathbf{A}_k^T \mathbf{H}_k^T]^T = n$, and rank $[\mathbf{A}_k \mathbf{D}_k]^T = n$. Here, $(\cdot)^T$ represents the matrix transpose and, as in Ref. 9, we define the relations $\mathbf{H}_k^T \mathbf{G}_k \equiv \mathbf{P}_k$ and $\mathbf{D}_k \mathbf{E}_k^T \equiv \mathbf{L}_k$.

Control Solution for a State-Dependent Linear-Quadratic Dynamic Game

It is well known that solving the linear-quadratic PSI dynamic game over a finite time horizon involves the solution of two generalized Riccati differential (difference) equations (GRDEs).[9,11,21] Here, we summarize the results and illustrate the online control computations that are performed at each sample-instant. We first define the discrete time-to-go variable s as $s \triangleq N - k$, where k and N, as previously defined, are the discrete time and terminal time variables, respectively. For notational convenience, we also define the following matrices.

$\bar{\mathbf{A}}_k \triangleq \mathbf{A}_k - \mathbf{B}_k \mathbf{R}_k^{-1} \mathbf{P}_k^T$	$\bar{\mathbf{Q}}_k \triangleq \mathbf{Q}_k - \mathbf{P}_k \mathbf{R}_k^{-1} \mathbf{P}_k^T$
$\tilde{\mathbf{A}}_k \triangleq \mathbf{A}_k - \mathbf{L}_k \mathbf{N}_k^{-1} \mathbf{C}_k$	$\Pi_k \triangleq \mathbf{D}_k \mathbf{D}_k^T - \mathbf{L}_k \mathbf{N}_k^{-1} \mathbf{L}_k^T$
$\mathbf{\Gamma}_k \triangleq \mathbf{M}_s^{-1} + \mathbf{B}_k \mathbf{R}_k^{-1} \mathbf{B}_k^T - \gamma^{-2} \mathbf{D}_k \mathbf{D}_k^T$	$\Delta_k \triangleq \mathbf{\Sigma}_k^{-1} + \mathbf{C}_k^T \mathbf{N}_k^{-1} \mathbf{C}_k - \gamma^{-2} \mathbf{Q}_k$
$\tilde{\mathbf{M}}_{s+1} \triangleq \bar{\mathbf{A}}_k^T (\mathbf{M}_s^{-1} - \gamma^{-2} \mathbf{D}_k \mathbf{D}_k^T)^{-1} \bar{\mathbf{A}}_k + \bar{\mathbf{Q}}_k$	$\tilde{\mathbf{\Sigma}}_{k+1} \triangleq \tilde{\mathbf{A}}_k (\mathbf{\Sigma}_k^{-1} - \gamma^{-2} Q_k)^{-1} \tilde{\mathbf{A}}_k^T + \Pi_k$.

(5)

For a given disturbance attenuation parameter γ satisfying $\gamma \geq \gamma^*$, the following steps are performed at each sample-instant:

1. Parameterize the nonlinear system described in Eq. 1 and subsequently discretize the state-dependent representation to obtain the discrete-time representation described by Eq. 3.
2. Propagate the following estimator GRDE (EGRDE) from discrete-time k to $k+1$:

$$\mathbf{\Sigma}_{k+1} = \tilde{\mathbf{A}}_k \Delta_k^{-1} \tilde{\mathbf{A}}_k^T + \Pi_k, \mathbf{\Sigma}_{k=0} = \mathbf{Q}_0^{-1} . \tag{6}$$

3. Solve the following control GRDE (CGRDE) to obtain M_{s+1}:

$$\mathbf{M}_{s+1} = \bar{\mathbf{A}}_k^T \mathbf{\Gamma}_k^{-1} \bar{\mathbf{A}}_k + \bar{\mathbf{Q}}_k, \mathbf{M}_{s=0} = \mathbf{Q}_f . \tag{7}$$

4. Compute the state estimates $\hat{\mathbf{x}}_k$ and control solution $\hat{\mathbf{u}}_k$ at time k according to the following set of equations:

$$\begin{aligned}
\bar{\mathbf{x}}_{k+1} &= \mathbf{A}_k \bar{\mathbf{x}}_k + \mathbf{B}_k \hat{\mathbf{u}}_k + \gamma^{-2} \tilde{\mathbf{A}}_k \Delta_k^{-1} \mathbf{H}_k^T \hat{\mathbf{z}}_k + (\tilde{\mathbf{A}}_k \Delta_k^{-1} \mathbf{H}_k^T + \mathbf{L}_k) \mathbf{N}_k^{-1} (\mathbf{y}_k - \mathbf{C}_k \bar{\mathbf{x}}_k), \ \bar{\mathbf{x}}_0 = \mathbf{0} \\
\hat{\mathbf{x}}_k &= [\mathbf{I} - \mathbf{\Sigma}_k (\gamma^{-2} \mathbf{M}_{s+1} - \mathbf{C}_k^T \mathbf{N}_k^{-1} \mathbf{C}_k)]^{-1} (\bar{\mathbf{x}}_k + \mathbf{\Sigma}_k \mathbf{C}_k^T \mathbf{N}_k^{-1} \mathbf{y}_k) \\
\hat{\mathbf{u}}_k &= -\mathbf{R}_k^{-1} (\mathbf{B}_k^T \mathbf{\Gamma}_k^{-1} \bar{\mathbf{A}}_k + \mathbf{P}_k^T)(\mathbf{I} - \gamma^{-2} \mathbf{\Sigma}_k \mathbf{M}_{s+1})^{-1} \hat{\mathbf{x}}_k \\
\hat{\mathbf{z}}_k &= \mathbf{H}_k \hat{\mathbf{x}}_k + \mathbf{G}_k \hat{\mathbf{u}}_k .
\end{aligned} \tag{8}$$

5. Repeat steps 1 through 4 at the estimator and control update rates.

In Eq. 8, $\hat{\mathbf{x}}_k$ represents the state-vector estimate at time k, taking into account measurements at time k. Note that the control $\hat{\mathbf{u}}_k$ *explicitly* accounts for estimation uncertainties as represented by the presence of the EGRDE term Σ_k. Therefore, we say that the control is *risk-averse*. Alternatively, if we had full state information (FSI), Σ_k is zero and the control solution $\hat{\mathbf{u}}_k$ collapses to the more familiar FSI form.

Some additional comments are in order. Unlike the typical RDE, a GRDE is one in which the sign of the quadratic term is a function of the disturbance attenuation variable γ. Hence, the existence of a solution to a GRDE is γ-dependent and the selection of γ is part of the design process. Generally, we desire the smallest possible γ that will still ensure solutions to the EGRDE and CGRDE. Assuming that γ has been chosen to satisfy $\gamma \geq \gamma^*$, the following conditions must also be satisfied:

$$\rho(\boldsymbol{\Sigma}_k \mathbf{Q}_k [\mathbf{I} + \boldsymbol{\Sigma}_k \mathbf{C}_k^T \mathbf{N}_k^{-1} \mathbf{C}_k]^{-1}) \boldsymbol{\Sigma}_k^{-1} < \gamma^{-2} \text{ and } \rho(\boldsymbol{\Sigma}_k \tilde{\mathbf{M}}_{s+1}) < \gamma^{-2} , \tag{9}$$

where $\rho(\cdot)$ denotes the spectral radius (maximum eigenvalue) of the argument.

The EGRDE, which is akin to the error covariance matrix in a discrete-time Kalman filter, is straightforward to solve (propagate) forward in terms of discrete-time k. In contrast to the EGRDE, the solution of the state-dependent CGRDE poses a challenge. The key issue is that, at the control update rate, the CGRDE must be solved backward from the terminal time N to the current time k to obtain a control solution at time k. The terminal penalty matrix $\mathbf{Q}_f$ serves as the boundary condition. If we assume the state trajectories over the solution interval $[k, N]$ are such that the (state-dependent) plant matrices remain approximately constant, then efficient solution methods can be applied. We simply mention here that we use the negative exponential matrix technique[24,25] to solve the CGRDE at the control solution rate.

Regarding implementation, two other comments are in order: (1) the estimator and control solution rates can, in general, differ, and (2) measurements (e.g., from dissimilar sensors) can enter the controller at differing rates. It is straightforward to extend the approach discussed above to handle these issues, but we do not address them in this article.

Approximation Error of the CGRDE Solution

The algorithm described above assumes constant plant matrices when solving the CGRDE (at each sample-instant); hence, some approximation error will result in the solution of the state-dependent CGRDE and, to a lesser extent, the EGRDE. Short of implementing the iterative procedure that would be necessary to precisely solve the actual state-dependent control solution, one can make a qualitative estimate of the approximation error when constant matrices are assumed. This has been done for the system we discuss in the next section by examining the sensitivity of the performance index, Eq. 4, with respect to deviations in the state trajectory. This sensitivity is central to the design of an optimal controller. Assuming constant plant matrices, we found that the initial rate of change of this value, with respect to time, differed minimally from that which would result when assuming varying plant matrices. These qualitative results add credence to the SDRDE technique as applied to this class of problems. The performance results we show later in the article further support this conclusion.

THE INTEGRATED PLANT MODEL

The PSI dynamic game formulation yields a coupling between estimation uncertainty and control action: the result is that *both* EGRDE and CGRDE solutions are required to compute the feedback control solution. This is in contrast to traditional feedback control algorithms wherein estimation uncertainty does not directly influence control action. In this section, we summarize the more explicit aspect of a fully integrated missile G&C system, namely, the appropriate definition of an integrated plant model. Therefore, we must define a suitable plant model, of the form shown in Eq. 1, that includes homing loop kinematics and target acceleration states (i.e., the guidance elements), missile dynamics, and other (possible) elements necessary to effectively perform the missile G&C task. Doing so provides an explicit coupling between the guidance and flight control functions. A derivation of the plant model and a discussion of why certain design choices were made are beyond the scope of this article but, for completeness, we outline the structure of the integrated plant model. The interested reader is referred to Refs. 4, 8, 18, and 19 for additional modeling details.

States, Measurements, Controls, and Performance Options

The reader is reminded of the plant structure illustrated in Eq. 1. Furthermore, recall that, once the model has been defined, it must be brought to the state-dependent form illustrated by Eq. 3. According to this structure, an overview of the state $\mathbf{x}(t)$, measurement $\mathbf{y}(t)$, control $\mathbf{u}(t)$, and performance output $\boldsymbol{z}(t)$ vectors is given in Eq. 10.

$$\mathbf{x}(t)=\begin{bmatrix} r_y^{\mathrm{G}}(t)\\ \dot{r}_y^{\mathrm{G}}(t)\\ r_z^{\mathrm{G}}(t)\\ \dot{r}_z^{\mathrm{G}}(t)\end{bmatrix}\}\text{relative kinematics}\quad \begin{bmatrix}\alpha(t)\\ \beta(t)\\ p(t)\\ q(t)\\ r(t)\\ \bar{\varphi}_{\mathrm{err}}(t)\end{bmatrix}\}\text{body motion}\quad \begin{bmatrix}\delta_r(t)\\ \dot{\delta}_r(t)\\ \delta_p(t)\\ \dot{\delta}_p(t)\\ \delta_y(t)\\ \dot{\delta}_y(t)\end{bmatrix}\}\text{actuator}\quad \begin{bmatrix} a_{T_y}^{\mathrm{G}}\\ a_{T_z}^{\mathrm{G}}\end{bmatrix}\}\text{target}$$

$$\mathbf{y}(t)=\begin{bmatrix} r_y^{\mathrm{G}}(t)\\ r_z^{\mathrm{G}}(t)\\ a_{m_y}(t)\\ a_{m_z}(t)\\ p(t)\\ q(t)\\ r(t)\\ \dot{\varphi}_{\mathrm{err}}(t)\\ \delta_r(t)\\ \delta_p(t)\\ \delta_y(t)\\ F_{x_0}(t)\\ g(t)\end{bmatrix}\qquad \mathbf{u}(t)=\begin{bmatrix}\delta_{r_c}(t)\\ \delta_{p_c}(t)\\ \delta_{y_c}(t)\end{bmatrix}\qquad \mathbf{z}(t)=\begin{bmatrix} r_y^{\mathrm{G}}(t)\\ \dot{r}_y^{\mathrm{G}}(t)\\ r_z^{\mathrm{G}}(t)\\ \dot{r}_z^{\mathrm{G}}(t)\\ \alpha(t)\\ \beta(t)\\ p(t)\\ q(t)\\ r(t)\\ \varphi_{\mathrm{err}}(t)\\ \delta_r(t)\\ \dot{\delta}_p(t)\\ \dot{\delta}_y(t)\\ \delta_{r_c}(t)\\ \delta_{p_c}(t)\\ \delta_{y_c}(t)\end{bmatrix} \tag{10}$$

States

Equation 10 highlights the fact that the state vector $\mathbf{x}(t)$ contains both guidance and missile dynamic states. For simplicity, a planar depiction of the homing geometry is shown in Fig. 4, where the target–missile relative positions in the *x*/*y* axis, $\{r_x^I, r_y^I\}$, are shown with respect to the inertial reference frame *I*. For our purposes, the guidance states are defined as target–missile relative positions, $\{r_y^{\mathrm{G}}, r_z^{\mathrm{G}}\}$; relative velocities, $\{\dot{r}_y^{\mathrm{G}}, \dot{r}_z^{\mathrm{G}}\}$; and target acceleration components, $\{a_{T_y}^{\mathrm{G}}, a_{T_z}^{\mathrm{G}}\}$, normal to an inertial (guidance) reference axis system. The superscript G indicates quantities with regard to the inertial guidance frame. A target acceleration model is defined in the guidance frame *y* and *z* axis as the first-order lag process shown below. In this model, τ_T represents the target maneuver time constant and $\omega_T(t)$ is a disturbance input.

$$\dot{a}_{T_i}^{\mathrm{G}}(t)=-\frac{1}{\tau_T}a_{T_i}^{\mathrm{G}}(t)+\frac{1}{\tau_T}\omega_T(t),\ i=y,z\,. \tag{11}$$

Figure 5 illustrates the missile body-axis system (the origin is the missile center of gravity) and many of the parameters necessary to describe missile body motion in this axis system. Assuming missile airframe *x*–*z* axis symmetry, and that the mass distribution is such that $I_{yy}=I_{zz}$, then the force and moment equations can be expressed as shown in Eq. 12 (Ref. 8):

$$\begin{aligned} \bar{F}_x &\triangleq F_x+W_x+T_x=m[\dot{u}+qw-rv] \\ \bar{F}_z &\triangleq F_z+W_z=m[\dot{w}-qu+pv] \\ \bar{F}_y &\triangleq F_y+W_y=m[\dot{v}-pw+ru] \end{aligned} \qquad \left| \qquad \begin{aligned} \mathrm{M}_x &= I_{xx}\dot{p} \\ \mathrm{M}_y &= I_{yy}\dot{q}+[I_{xx}-I_{zz}]pr \\ \mathrm{M}_z &= I_{zz}\dot{r}+[I_{yy}-I_{xx}]pq\,. \end{aligned} \right. \tag{12}$$

The boxed insert lists the defining terms, where we note that t_x, c_x, and s_x denote tan(*x*), cos(*x*), and sin(*x*), respectively. According to Eq. 10, 12 missile dynamic states are defined: AoA (α), AoS (β), body rates (*p*, *q*, *r*), roll

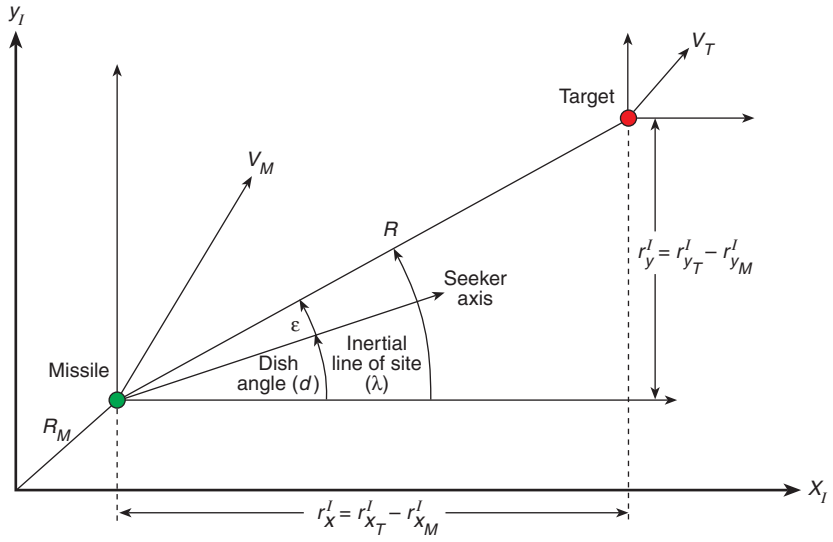

Figure 4. Planar depiction of the relative homing geometry. In many guidance systems, the target–missile relative positions, velocities, and accelerations are used to make guidance decisions. Here, the target–missile relative positions with respect to an inertial frame are shown for each axis. Differentiation of these terms produces relative velocity in each axis; double-differentiation yields relative acceleration.

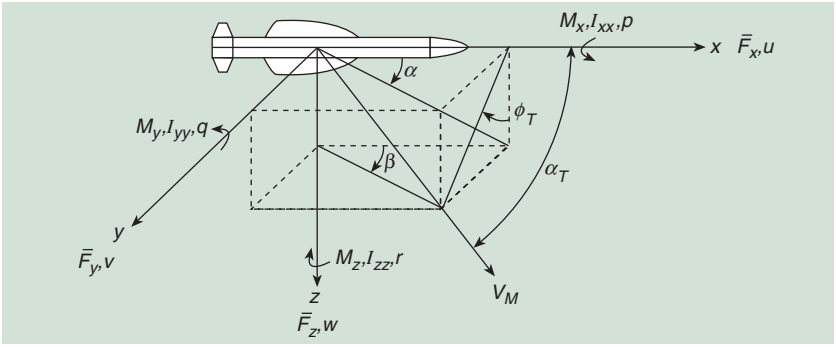

Figure 5. The origin of the body-fixed coordinate system is at the missile center of gravity. The forces and moments acting on the missile, as well as other relevant aerodynamic quantities, are shown with respect to this coordinate system.

VEHICLE FORCE, MOMENT, AND MOTION/ORIENTATION TERMS

$\bar{F}_i$	Total force component in $i = \{x, y, z\}$ body axis
F_i	Aerodynamic force component in $i = \{x, y, z\}$ body axis
W_i	Weight component in $i = \{x, y, z\}$ body axis
M_i	Aerodynamic moment component about $i = \{x, y, z\}$ body axis
T_x	Thrust in x body axis
$\{u, v, w\}$,	Velocity components in $i = \{x, y, z\}$ body axis
$\{p, q, r\}$	Angular rates about $\{x, y, z\}$ body axis
m, I_{ii}	Vehicle mass and moment of inertia in $\{x, y, z\}$ body axis
$\alpha = \tan^{-1}(w/u)$	Angle of attack (AoA)
$\beta = \tan^{-1}(v/u)$	Angle of sideslip (AoS)
$\alpha_T = \tan^{-1}(\sqrt{v^2 + w^2}/u^2)$	Total AoA
$\phi_T = \tan^{-1}(v/w)$	Total roll angle
$V_M = [u^2 + v^2 + w^2]^{1/2}$	Velocity magnitude
$\dot{\theta} = qc_\phi - rs_\phi$	
$\dot{\phi} = p + qs_\phi t_\theta + rc_\phi t_\theta$	Euler angle equations
$\dot{\psi} = q\frac{s_\phi}{c_\theta} + r\frac{c_\phi}{c_\theta}$	

error ($\bar{\varphi}_{\text{err}}$), pitch-yaw-roll tail-fin angular positions ($\delta_i, i = p, y, r$), and tail-fin angular rates ($\dot{\delta}_i, i = p, y, r$). (With regard to tail-fin notation, (p, y, r) refers to pitch-yaw-roll fin deflection and is not to be confused with missile body rate definitions.) Given these definitions, the state dynamics can be written as

$$\dot{\alpha} = \frac{\bar{F}_z Q_{\alpha,\beta} c_\alpha^2}{mV_M} - \frac{\bar{F}_x Q_{\alpha,\beta} c_\alpha s_\alpha}{mV_M} + q - [p + rt_\alpha] t_\beta c_\alpha^2$$

$$\dot{\beta} = \frac{\bar{F}_y Q_{\alpha,\beta} c_\beta^2}{mV_M} - \frac{\bar{F}_x Q_{\alpha,\beta} c_\beta s_\beta}{mV_M} - r + [p + qt_\beta] t_\alpha c_\beta^2 \tag{13}$$

$$\dot{p} = \frac{M_x}{I_{xx}},\ \dot{q} = \frac{M_y}{I_{yy}} - \frac{I_{xx} - I_{zz}}{I_{yy}} pr,\ \dot{r} = \frac{M_z}{I_{zz}} - \frac{I_{yy} - I_{xx}}{I_{zz}} pq \tag{14}$$

$$\dot{\bar{\varphi}}_{\text{err}}(t) = \frac{1}{\tau_\varphi} \underbrace{\{\dot{\varphi}_{\text{cmd}}(t) - [p(t) + q(t) s_\varphi t_\theta + r(t) c_\varphi t_\theta]\}}_{\dot{\varphi}_{\text{err}}} - \frac{1}{\tau_\varphi} \bar{\varphi}_{\text{err}}(t) \tag{15}$$

$$\ddot{\delta}_i(t) = -2\xi\omega_n \dot{\delta}_i(t) + \omega_n^2 [\delta_{i_c}(t) - \delta_i(t)],\ i = p, y, r\ . \tag{16}$$

In Eq. 15, $\dot{\varphi}_{\text{cmd}}$ is the commanded Euler roll angle rate and τ_ϕ is an adjustable parameter. In Eq. 16, δ_{i_c} represents the commanded pitch-yaw-roll angular tail-fin position, while ω_n and ξ represent the natural frequency and damping ratio of the tail-fin servo-actuator, respectively.

Measurements

With reference to the measurement vector $\mathbf{y}(t)$ in Eq. 10, the guidance measurements are the first two entries. Missile lateral accelerometer and rate gyro measurements follow. The derivative of roll error $\dot{\phi}_{\text{err}}$ (see Eq. 15) is also defined as a measurement. This approach facilitates injection of a desired missile roll orientation into the system. Tail-fin angle measurements are also assumed to be available. Finally, note that the measurement vector entries $F_{x_0}(t)$ and $g(t)$ are defined as *pseudo-measurements* to account for axial thrust-minus-drag and gravity, respectively. Referring to Eq. 3, these pseudo-measurements influence the plant state dynamics through the process and measurement disturbance matrices $\mathbf{D}(t)(\mathbf{D}_k)$ and $\mathbf{E}(t)(\mathbf{E}_k)$, respectively.

Controls and Performance Outputs

With reference to Eqs. 10 and 16, the IGC control vector $\mathbf{u}(t)$ comprises the three tail-fin angular position commands. This is typical for tail-controlled missiles.

Given the state and control definitions, the performance output vector $\mathbf{z}(t)$ contains the elements necessary to specify IGC performance, i.e., relative kinematic states in addition to missile dynamic states and control signals. Notice that we have included the relative velocity states in the performance output. Although these components are not critical to our problem, they allow additional flexibility to define IGC guidance performance.

Coupling of the Guidance States with Missile State Dynamics

Referring again to the planar depiction of the homing geometry of Fig. 4, consider the expression for target–missile relative acceleration (normal to the reference) given as

$$\{\ddot{r}_y^G, \ddot{r}_z^G\} = \{a_{T_y}^G - a_{M_y}^G, a_{T_z}^G - a_{M_z}^G\} . \tag{17}$$

We integrate this equation twice to obtain relative position. Minimization of the target–missile relative position (in the guidance frame) is a principal goal of the guidance system. The guidance system attempts to do this by commanding interceptor maneuvers.

As we indicated above, the traditional (decoupled) architecture separates guidance and flight control functions (Fig. 1). Because this connection has been "broken," the decoupled guidance system designer must make assumptions regarding how the missile will respond to acceleration commands. Figure 6 illustrates a typical guidance model used for (decoupled) guidance law design. The model assumes that the interceptor response from commanded to achieved acceleration can be represented as a first-order lag. Recall that Fig. 3 compared this lag-response model to a "true" tail-controlled missile response and showed that the accuracy of this assumption degrades as the homing time approaches zero. Consequently, during the final critical (tens to hundreds of) milliseconds of the engagement, the interceptor will, momentarily, respond in the wrong direction, and guidance accuracy can suffer as a result.

In contrast to the decoupled approach, the IGC relative acceleration model is much more accurate. To show this quantitatively would require combining the results of Eq. 8 with the dynamic equations of motion implied by the structure shown in Eq. 10 and subsequently replacing the missile response model in Fig. 6 with something far more complex. The result is that an IGC system generates guidance decisions that are substantially more precise as the homing time approaches zero (Fig. 3). Thus, it is more likely to command acceleration appropriately, thereby minimizing the final miss distance. The performance results we present later bear this out.

State Factorization

To accommodate the SDRDE solution methodology, a viable factorization of the system states is necessary. Toward this end, one can express the missile forces and moments—F_i, M_i, $i = \{x, y, z\}$—as functions of the states α, β, and δ_i, $i = \{p, y, r\}$, which results in the following expressions.

$$\begin{bmatrix} F_x \\ F_y \\ F_z \\ M_x \\ M_y \\ M_z \end{bmatrix} = \begin{bmatrix} f_{x_\alpha} & f_{x_\beta} & f_{x_{\delta_p}} & f_{x_{\delta_y}} & f_{x_{\delta_r}} \\ f_{y_\alpha} & f_{y_\beta} & f_{y_{\delta_p}} & f_{y_{\delta_y}} & f_{y_{\delta_r}} \\ f_{z_\alpha} & f_{z_\beta} & f_{z_{\delta_p}} & f_{z_{\delta_y}} & f_{z_{\delta_r}} \\ m_{x_\alpha} & m_{x_\beta} & m_{x_{\delta_p}} & m_{x_{\delta_y}} & m_{x_{\delta_r}} \\ m_{y_\alpha} & m_{y_\beta} & m_{y_{\delta_p}} & m_{y_{\delta_y}} & m_{y_{\delta_r}} \\ m_{z_\alpha} & m_{z_\beta} & m_{z_{\delta_p}} & m_{z_{\delta_y}} & m_{z_{\delta_r}} \end{bmatrix} \begin{bmatrix} \alpha \\ \beta \\ \delta_p \\ \delta_y \\ \delta_r \end{bmatrix} . \tag{18}$$

As an example, the roll rate expression in Eq. 14 is parameterized below:

$$\dot{p} = \frac{m_{x_\alpha}\alpha + m_{x_\beta}\beta + m_{x_{\delta_p}}\delta_p + m_{x_{\delta_y}}\delta_y + m_{x_{\delta_r}}\delta_r}{I_{xx}} . \tag{19}$$

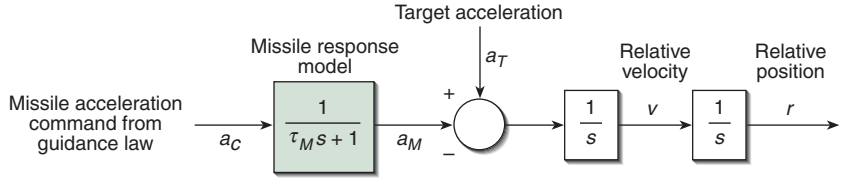

Figure 6. The homing-loop kinematics model, typically used for decoupled guidance system design, is described by this figure. The model assumes that the interceptor response from commanded to achieved acceleration can be represented as a first-order lag.

The expressions shown in Eq. 18 are used in the plant model wherever force and/or moment entries appear (e.g., Eqs. 13 and 14).

IGC Performance Specification

The objective is to obtain a design that minimizes a given performance index under the worst possible disturbances or parameter variations that maximize the same performance index. Below we repeat the soft-constrained dynamic game problem given earlier for the sake of discussion.

$$\min_{\mathbf{u}_k}\max_{\mathbf{w}_k} J_\gamma(\mathbf{u}_k, \mathbf{w}_k) = |\mathbf{x}_N|^2_{\mathbf{Q}_f} - \gamma^2 |\mathbf{x}_0 - \hat{\mathbf{x}}_0|^2_{\mathbf{Q}_0} + \sum_0^{N-1} \{|\mathbf{z}_k|^2 - \gamma^2 |\mathbf{w}_k|^2\}$$

$$\text{Subject to} \quad \begin{aligned} \mathbf{x}_{k+1} &= \mathbf{A}_k\mathbf{x}_k + \mathbf{B}_k\mathbf{u}_k + \mathbf{D}_k\mathbf{w}_k \\ \mathbf{y}_k &= \mathbf{C}_k\mathbf{x}_k + \mathbf{E}_k\mathbf{w}_k \\ \mathbf{z}_k &= \mathbf{H}_k\mathbf{x}_k + \mathbf{G}_k\mathbf{u}_k \,. \end{aligned} \tag{20}$$

Regarding this specification, we adjust entries of the $\mathbf{D}_k$, $\mathbf{E}_k$, $\mathbf{G}_k$, $\mathbf{H}_k$, $\mathbf{Q}_0$, and $\mathbf{Q}_f$ matrices to elicit a desired overall performance. Process and measurement disturbance matrices, $\mathbf{D}_k$ and $\mathbf{E}_k$, respectively, are initially set according to expected (or assumed) levels of (process and measurement) disturbances entering the system. The entries can be adjusted as needed to fine-tune overall controller performance.

For our problem, the terminal penalty weighting matrix $\mathbf{Q}_f$ is adjusted to adequately penalize the final miss distance. Hence, the only non-zero elements are those diagonal entries related to the relative position states. Clearly, relative position at the closest point of approach (CPA) *is* the final miss distance. Note that we can generally specify $\mathbf{Q}_f$ to satisfy a much broader goal than simply minimizing final miss distance. For example, we can specify a desire to keep missile body (rotation) rates "small" at intercept in addition to minimizing final miss. This additional specification could contribute to improving the P_k for interceptors that rely on a fuzing system and a directional fragmentation warhead. In any event, some "trade-off" in performance must be expected when multiple endgame conditions are specified.

Matrix $\mathbf{Q}_0$ is analogous to the initial covariance matrix in a Kalman filter setting[3] and should be set to represent the assumed initial condition/estimation uncertainties.

For the performance index, the contributors under the summation (in Eq. 20) are the performance output matrices $\mathbf{H}_k$ and $\mathbf{G}_k$. Specification of these entries will affect interceptor behavior throughout the engagement. Non-zero entries of the control performance matrix $\mathbf{G}_k$ are adjusted to penalize control effort (i.e., commanded tail-fin angular positions) under the summation. Non-zero entries of the state performance matrix $\mathbf{H}_k$ are specified to penalize the contribution of individual states under the summation. For example, the roll error state ϕ_{err} is penalized throughout the flight to achieve/maintain a desired roll configuration.

In a tactical design, the G&C system must operate over a wide range of flight conditions, threat behaviors, and engagement geometries. In general, this implies that many of the G&C design parameters evolve nonlinearly as functions of certain system states and/or other exogenous variables like dynamic pressure and altitude. However, since a quasi-linear design problem is more desirable, the performance envelope must be partitioned into subregions, and many of the adjustable parameters for each subregion designed (tuned). The individual designs are then scheduled as the engagement evolves. This procedure is discussed further under "Simulation-Based Performance Optimization."

Limiting the Commanded Acceleration

The maximum allowable interceptor lateral acceleration must be limited to avoid structural damage or for stability reasons. In a decoupled system, the commanded missile acceleration coming from the guidance law is limited prior to autopilot input. Thus, if the autopilot has been properly designed, when acceleration limiting takes place the missile will exhibit little overshoot beyond allowable levels. In a fully integrated system, however, there is no guidance and flight control component separation. Thus, an alternative acceleration limiting function was developed.[18] As illustrated in Fig. 7, IGC fin commands δ_{cmd} are first mapped into equivalent acceleration commands a_{cmd}. This is done using relevant sensor measurements and IGC state estimates and by interrogating the aerodynamic database to estimate the appropriate coefficients. The mapped acceleration commands are then limited (if necessary), yielding $\tilde{a}_{\text{cmd}}$. The limited acceleration commands are subsequently mapped back to equivalent IGC fin commands $\tilde{\delta}_{\text{cmd}}$ and passed to the steering control section.

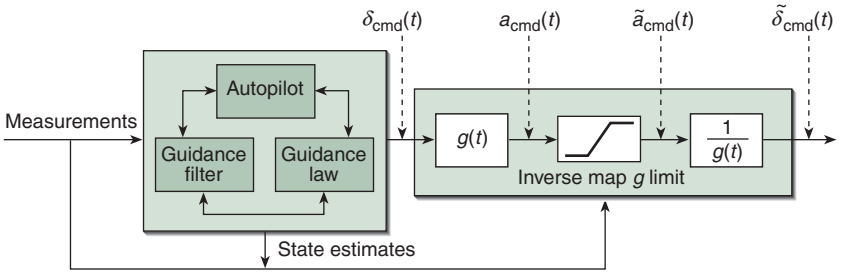

Figure 7. Inverse map acceleration limiting used in the IGC prototype design. An external acceleration limit function was developed for the design. This function dynamically maps tail-fin angular position commands coming from the IGC into equivalent lateral acceleration commands in the missile body frame. The acceleration commands can thus be limited (if necessary) and dynamically mapped back to equivalent tail-fin position commands. Here, $g(t)$ represents functional mapping.

SIMULATION-BASED PERFORMANCE OPTIMIZATION

Despite the diversity and complexity of modern G&C synthesis techniques and algorithms, some common features emerge. Many are multivariable techniques that consider high-order plant models for design purposes. Furthermore, additional sensors are often required to support algorithm operation. These factors contribute to the complexity of the algorithms, thereby imposing particular challenges during the algorithm performance optimization, or tuning, stage. This problem of scale makes conventional "analyze and iterate" or "hand-tuning" methods difficult (at best) and motivates the use of the computer to iteratively seek the "best" solution. That is certainly the case here. Plant order and overall IGC algorithm complexity lead to a large number of tuning parameters. Previously, we identified the relevant (high-order) matrices that must be designed (tuned) appropriately. In addition, the inherent coupling between G&C components complicates things further. For these reasons, we will avoid using conventional methods for optimizing guidance, navigation, and control performance (tuning) in favor of an automated, simulation-based performance optimization technique.

Reference 26 describes the simulation-based optimization technique that we use. A comprehensive six-degree-of-freedom (6-DOF) terminal homing simulation is employed to adjust (tune) a number of IGC matrices over the engagement space. The core of our approach is the simultaneous perturbation stochastic approximation (SPSA) algorithm.[27–29] First, a desired cost function is specified (not to be confused with the dynamic game performance index shown in Eq. 4). The SPSA algorithm uses noisy cost function "measurements," generated by the 6-DOF simulation, to approximate the cost function gradient with respect to the design parameters. This gradient approximation drives the design parameters toward their optimum values.

As mentioned, SPSA use necessitates the specification of a scalar-valued cost function that will drive the tuning process. We define the cost to be a weighted sum of the final miss distance (CPA) in feet and a measure of fin activity (FA) over the flight time. To obtain FA, the pitch, yaw, and roll tail-fin angular accelerations are squared, integrated, and summed. CPA and FA are weighted to contribute approximately 95% and 5%, respectively, to the overall cost. Because the G&C algorithms must operate against a wide array of threats over a variety of flight conditions, use of the cost function should be carefully considered so as to capture the diversity of the operating requirements. To this end, the weighted sum of CPA and FA is averaged over a number of differing engagements. These engagements represent a variety of conditions such as missile and target initial geometries and target behavior (e.g., acceleration level and maneuver period), angles of attack and sideslip, dynamic pressure, etc.

The key performance optimization parameter classes present in the IGC system are process and measurement disturbance weights, $\mathbf{D}_k$ and $\mathbf{E}_k$, respectively; performance output weights $\mathbf{G}_k$ and $\mathbf{H}_k$; a small number of plant modeling parameters found in $\mathbf{A}_k$, $\mathbf{B}_k$, and $\mathbf{C}_k$; and initial condition and terminal state weighting matrices, $\mathbf{Q}_0$ and $\mathbf{Q}_f$, respectively. The significant tuning parameters are notionally shown in Fig. 8 and are those adjusted by the SPSA (optimization) algorithm for this study.

SIMULATION RESULTS

Six-Degree-of-Freedom Simulation Tool

We have employed a 6-DOF terminal homing Monte Carlo simulation for system performance optimization and analysis. This comprehensive tool incorporates a generic (realistic), fully coupled, nonlinear aerodynamics model (via table lookup); structural filtering; and fin command processing delays. The simulated endo-atmospheric interceptor is a body-dorsal-tail, skid-to-turn configuration (see Fig. 5, a notional missile drawing) that uses an active RF sensor for terminal homing. It has tail-only control (no sidethrusters or canards). A lethality enhancement device (warhead with a specified lethal radius) is necessary to effectuate a high P_k. (We assume here that any terminal miss within a specified lethal radius is an effective kill, but minimum miss is desired.) The inertial measurement unit gyro and accelerometer models include second-order dynamics, additive Gaussian noise, scale factor, and misalignment errors, and the gyro model includes a drift component. Tail-fin actuators are modeled as having second-order dynamics with

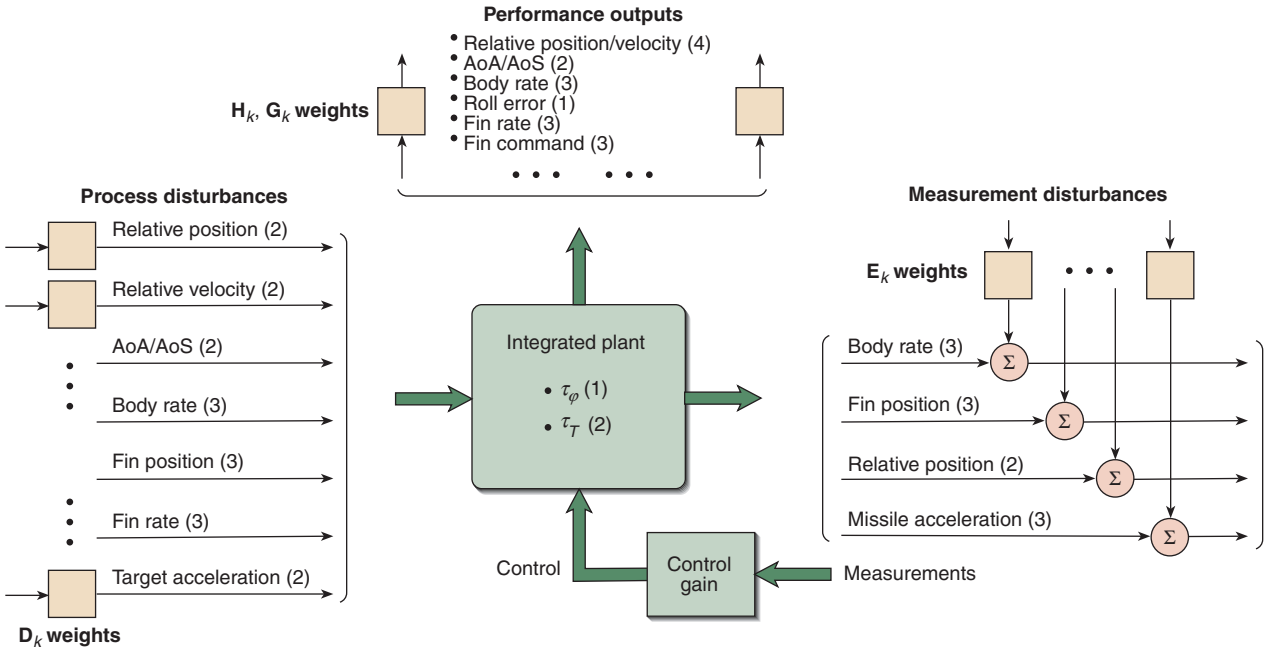

Figure 8. IGC tuning structure. All of the principal (first-order) tuning parameter classes (e.g., body rates) necessary to optimize IGC performance are indicated in the figure. Numbers in parentheses indicate the number of parameters within the specified class. These tuning parameters are adjusted using a stochastic gradient approximation algorithm in conjunction with a six-degree-of-freedom simulation.

fin rate and position limits. The RF sensor (seeker) angle measurements are corrupted by glint noise, radome-induced boresight errors (via table lookup), and angle noise consistent with an active RF seeker. Gaussian noise is added to true range and range rate to form range and range-rate measurements. The simulation includes a tactical ballistic missile (TBM) target generator that models ballistic slowdown and coning with variable acceleration capabilities and maneuver periods.

Benchmark G&C System

For comparison purposes, a benchmark G&C system was also designed. The benchmark concept is a decoupled architecture: guidance filter, guidance law, and autopilot components were developed. The guidance law is an optimal guidance formulation of the non-ideal pursuer-evader variety.[4] Dual three-state Kalman filters were designed for guidance filtering in the guidance frame y/z axis. Guidance states are relative position/velocity and target acceleration in each plane.[3] A two-timescale dynamic inversion autopilot was used.[7] As compared with a traditional three-loop design, this autopilot is, in general, easy to modify and provides very good (fast) performance. Note that, to ensure an equitable comparison, the benchmark system was tuned using the same automated technique used to tune the IGC system.

Monte Carlo Performance Comparison

To illustrate terminal homing IGC performance versus the benchmark system, we consider five TBM intercept scenarios with intercept altitudes in the 70- to 80-kft range. Some of the relevant engagement characteristics are given in Table 1. First, note that the threat lateral-maneuver acceleration levels increase with engagement number. Engagement 1 has no threat coning motion and therefore maneuver period is not applicable. Terminal homing times vary from about 5.4 to 6.6 s. We define heading error as the angle between the actual initial interceptor velocity vector and an initial velocity vector that would be necessary for a perfect intercept. This is a "rollup" measure of midcourse (flyout) guidance errors prior to terminal homing. All performance results are based on 200-run Monte Carlo sets.

Figure 9 shows cumulative miss distance statistics for all five engagements. Better performance is indicated by plot lines farther to the left and more vertical. As

Table 1. Threat-relevant engagement specifications.

	Homing time (s)	Maneuver period (s)	Maneuver level (g's)	Heading error (deg)
Engagement 1	6.6	n/a	0.0	1.4
Engagement 2	6.4	2.5	1.5	1.8
Engagement 3	6.5	2.0	3.5	1.7
Engagement 4	6.1	2.5	4.2	1.3
Engagement 5	5.4	2.0	4.2	1.5

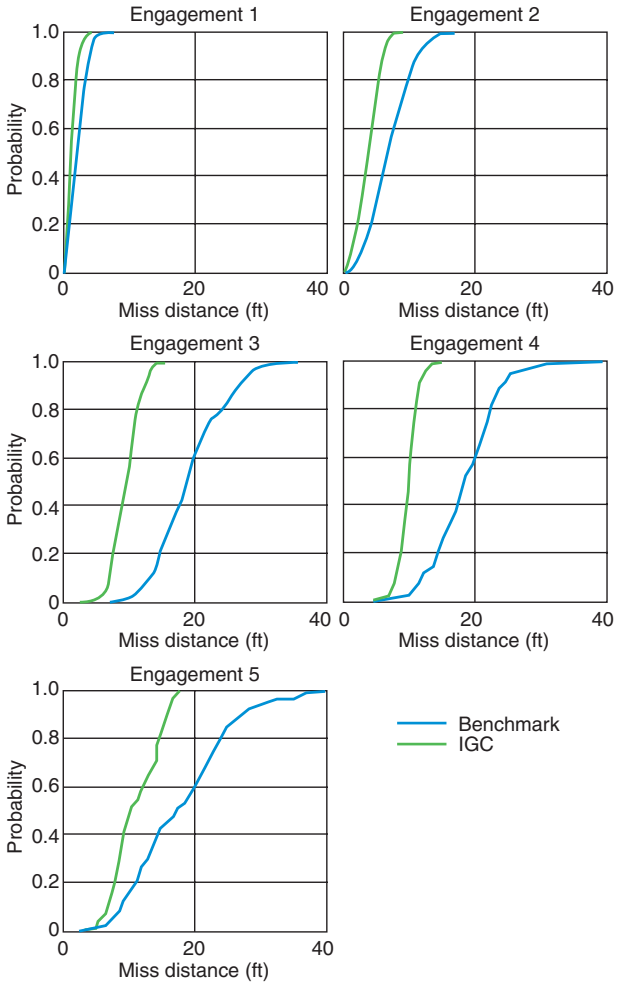

Figure 9. Cumulative probability miss distance comparisons. A cumulative probability miss distance chart is an effective way to visualize guided missile system performance in a Monte Carlo sense. A number of Monte Carlo simulation runs are made and the miss distances are logged for each run. Miss distance is read on the abscissa versus the probability of achieving a specified miss on the ordinate. Better performance is indicated by plot lines that are farther to the left and more vertical. Engagement 1 presents the least challenge to both systems because there is no threat coning motion, and the IGC system performs roughly 40% better in both mean miss and standard deviation of miss. For the other four engagements, which include increasing levels of threat coning motion (more stressing), the performance advantage offered by the IGC system becomes more dramatic.

expected, Engagement 1 presents the least challenge to both systems because there is no threat coning motion (i.e., no lateral maneuver). Both systems perform well in this case, with the IGC system roughly 40% better in both mean miss and standard deviation of miss. (The miss standard deviation measure illustrates that IGC performs more consistently than the benchmark system.) For the other four engagements, which include various levels of threat coning motion, the performance separation becomes even more evident.

Table 2 summarizes the performance results. The IGC system achieves a 40 to 50% improvement in mean miss and a 40 to 70% improvement in miss standard deviation versus the benchmark system. It is also interesting to note that the IGC performance advantage does not come at the expense of increased control energy, represented by the FA measure. Regarding FA, the IGC system exhibits a lower mean for all five engagements. However, the IGC tends to produce a wider spread of control energy values over a Monte Carlo set (i.e., a higher standard deviation). The IGC control energy measure tends to stay relatively low versus the benchmark system until the last few missile time constants prior to intercept. Within this endgame region, IGC behavior tends to cause a "leap" in commanded fin position to null out the remaining miss distance. On the other hand, the control energy measure for the benchmark system tends to increase linearly throughout the flight, with less rapid increase at the end. This is one indirect indicator of why the benchmark miss statistics are not as good as the IGC system.

Similarly, the IGC performance advantage does not come at the expense of a marked increase in commanded interceptor acceleration (at this altitude regime, the airframe was specified to have a maximum lateral acceleration capability of 20 *g*). In Table 2, the peak acceleration figure of merit represents the peak acceleration experienced by the airframe during terminal homing (this peak usually occurs very close to intercept). The peak acceleration statistics indicate that the IGC system required about 25% less acceleration, on average, versus the benchmark system. As with the FA figure of merit, the IGC system tends to have a larger standard deviation but a lower mean.

Parametric Sensitivity Comparisons

Table 1 listed the specific ranges of key engagement and threat characteristics that the IGC and benchmark systems were designed to accommodate: e.g., homing time, threat lateral maneuver level and period, and heading error at handover to terminal homing. To investigate system performance outside these "design-to" regions, we parametrically varied each threat-relevant engagement characteristic through extended but reasonable ranges. Engagement 1 served as the starting point for each parametric sweep. Mean miss statistics were computed using 100-run Monte Carlo sets. Figure 10a illustrates mean miss distance as a function of threat lateral maneuver level. Here, as threat lateral acceleration increases, IGC mean miss degrades more gracefully compared to the benchmark system. Note that this trend is evident in Table 2 for the baseline engagements but is more pronounced outside the baseline design region, i.e., as the threat becomes more stressing in terms of acceleration capability, the performance advantage afforded by the IGC system becomes more obvious.

Figure 10b illustrates percent improvement in IGC system mean miss distance versus the benchmark system

Table 2. Performance comparison statistics.

		Miss		Fin activity		Peak acceleration	
		Mean	SD	Mean	SD	Mean	SD
Engagement 1	Bechmark	2.2	1.3	1.1	0.2	5.5	2.2
	IGC	1.3	0.8	1.0	0.4	4.0	1.4
	% improvement	38.6	38.0	5.6	−52.9	27.1	33.8
Engagement 2	Benchmark	7.1	3.3	1.4	0.2	12.9	3.5
	IGC	3.9	1.8	1.0	0.3	8.1	3.2
	% improvement	45.0	46.4	30.1	−36.7	37.1	8.6
Engagement 3	Benchmark	19.3	5.4	1.6	0.2	17.1	2.1
	IGC	9.4	2.1	1.1	0.3	13.2	3.4
	% improvement	51.1	60.4	33.1	−45.6	22.6	−62.1
Engagement 4	Benchmark	18.4	5.3	1.3	0.1	18.4	2.0
	IGC	9.8	1.5	1.0	0.3	14.3	2.9
	% improvement	46.6	70.9	20.5	−162.5	22.0	−50.1
Engagement 5	Benchmark	17.8	7.7	1.2	0.1	18.8	1.9
	IGC	11.1	3.5	1.1	0.3	14.2	3.0
	% improvement	37.9	54.2	6.5	−187.5	24.5	−58.5

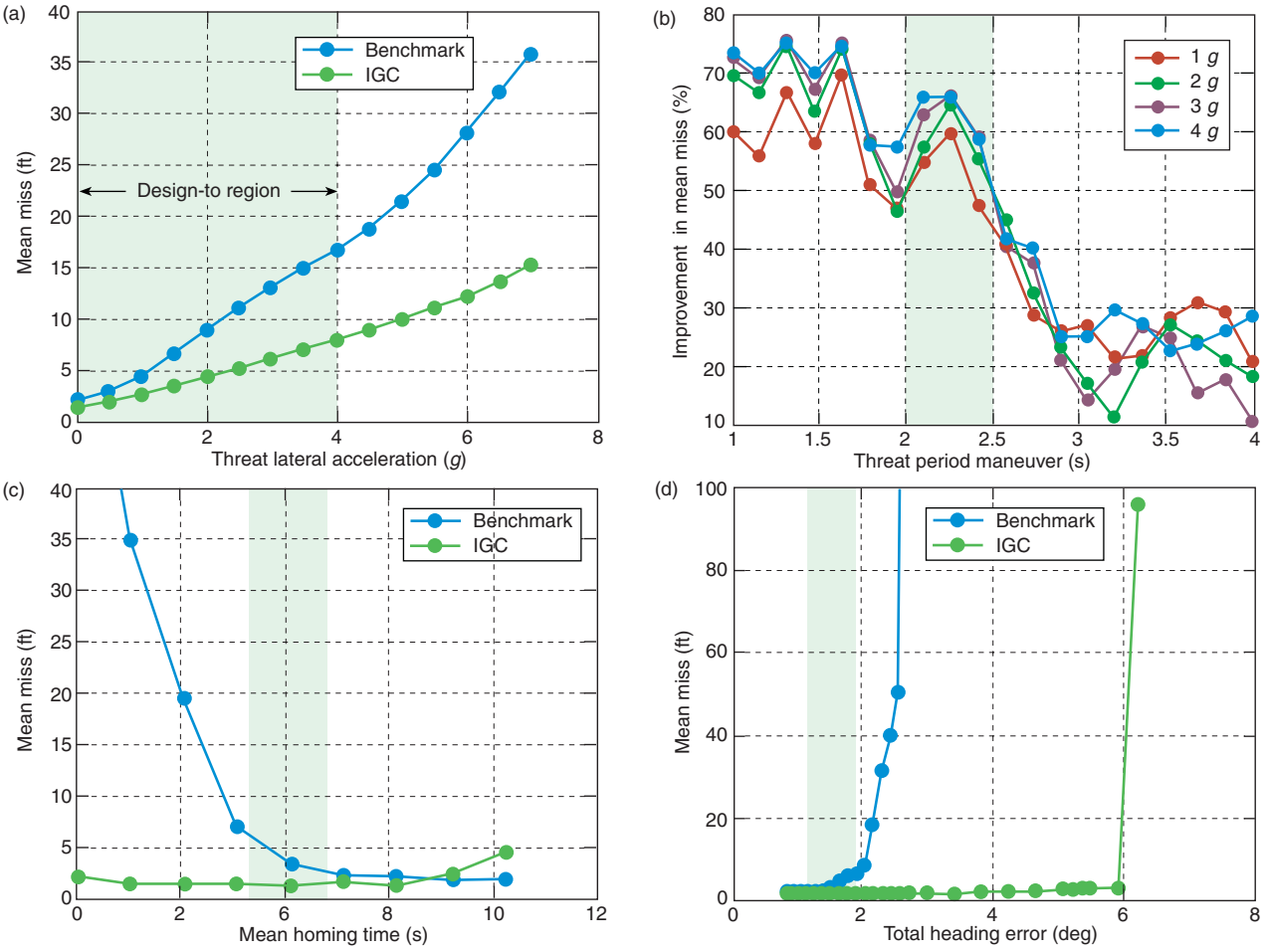

Figure 10. Parametric sensitivity comparisons. A number of Monte Carlo parametric sensitivity studies were conducted, including sensitivity to (a) threat lateral acceleration level, (b) threat maneuver period, (c) terminal homing time, and (d) heading error at the start of terminal homing. The shaded areas indicate the "design-to" regions for the benchmark and IGC systems. The results indicate that the IGC system performance advantage becomes even more evident as the engagement becomes more stressing. The IGC system performance also degrades more gracefully than does the benchmark system.

as the threat maneuver period varies: threat maneuver levels of 1 to 4 *g* are shown. For the range of maneuver periods considered here, shorter periods tend to offer more challenge. Again, we observe that the IGC performance advantage is substantial.

A mean miss distance versus homing time comparison is shown in Fig. 10c. Here, IGC performance is rather insensitive to homing time, whereas the benchmark system performance degrades rapidly for homing times shorter than those considered in the baseline design region. Likewise, in Fig. 10d, mean miss distance performance for the benchmark system degrades more rapidly for handover heading errors outside the design-to region, whereas IGC performance stays relatively consistent.

Clearly, these results could vary if the design regions were expanded and the systems were retuned to account for more diverse operating conditions. Nevertheless, given the equitable tuning approach and engagement characteristics considered here, the parametric sensitivity sweeps paint a consistent picture: the IGC performance advantage grows as the engagements become more stressing, and IGC performance degrades more gracefully outside the design-to region boundaries.

CLOSING REMARKS

Threat missile systems continue a steady evolution in technical sophistication, leading to increased capability and, consequently, the ability to perform a wider, deadlier, range of missions. The diversity of these threat missile systems and missions poses a significant challenge to missile interceptor design. This underscores the need for an *integrated* approach to missile interceptor design. Undoubtedly, technical advances in the various interceptor elements (e.g., airframe, actuation, sensor and propulsion systems) are, and will continue to be, necessary. It is the aggregate capability of these subsystems that defines the maximum performance potential of the interceptor. Nevertheless, optimal integration of the interceptor subsystems must still be accomplished, and this is the central role of the G&C system. In this article, we have discussed one such advanced G&C concept and IGC system. The IGC paradigm facilitates a level of synergism between interceptor flight control and guidance systems that is difficult to emulate within the traditional (decoupled) framework. Just as noteworthy, IGC presents a unified approach to interceptor performance optimization versus the traditional decoupled approach. Consequently, we believe the IGC paradigm is a critical step toward optimal interceptor design.

Modern missile interceptor G&C systems must, and will, continue to evolve to meet the challenges of next-generation threats. Hence, the complexity of these algorithms will grow as well. This fact presents a significant challenge to the designer during the algorithm performance optimization (tuning) stage. This problem of scale renders the traditional tuning methods difficult and motivates the use of the computer to iteratively seek the "best" solution. Here, we have discussed the application of the SPSA technique to simulation-based performance optimization of complex G&C algorithms. The efficacy of a simulation-based approach to G&C algorithm performance optimization was demonstrated by applying the SPSA technique to two algorithms: the IGC system and a dynamic inversion autopilot coupled with a Kalman filter and optimal guidance law. This approach has proven to be an effective tool for the task, as indicated by the results presented here.

For the prototype IGC system, the design objectives were to find a controller that minimizes the final miss distance and to control energy under worst-case target maneuver process and measurement disturbances. Performance of the prototype IGC system was compared to another high-performance, albeit decoupled, G&C system in a comprehensive 6-DOF terminal homing simulation tool. It was shown that the IGC system significantly improved the mean and standard deviation of the final miss distance, particularly against stressing threats. What is more, through parametric studies, it was shown that the IGC performance advantage continues to be evident as the engagements become more stressing and that IGC performance degrades more gracefully outside the design-to region boundaries.

Many interceptors use a lethality enhancement device to improve P_k. For example, endo-atmospheric guided missiles typically employ a fuzing system and fragmentation warhead to accomplish this. The performance of these lethality enhancement systems can be sensitive to endgame conditions. Suitably controlling the terminal interceptor body rates, interceptor-threat approach angles, etc., can help maximize the performance and effectiveness of the lethality enhancement device. Decoupled guidance systems do not have explicit "tuning knobs" to accomplish this. Instead, they are adjusted in an *ad hoc* (indirect) fashion in an attempt to improve endgame conditions. In contrast, an IGC paradigm can accommodate these types of performance criteria explicitly. In the future, we will extend the IGC control objectives to account for (and control) additional engagement parameters such as terminal threat-interceptor approach angle and interceptor body rates at intercept. The goal is explicit specification of endgame objectives leading to direct control of endgame behavior in a way that optimizes usage of the lethality enhancement device.

REFERENCES

[1]Witte, R. W., and McDonald, R. L. "Standard Missile: Guidance System Development," *Johns Hopkins APL Tech. Dig.* **2**(4), 289–298 (1981).

[2]Bar-Shalom, Y., Li, X. R., and Kirubarajan, T., *Estimation with Applications to Tracking and Navigation*, Wiley and Sons Publishers (2001).

[3]Grewal, M. S., and Andrews, A. P., *Kalman Filtering Theory and Practice*, Prentice Hall (1993).
[4]Ben-Asher, J. Z., and Yaesh, I., *Advances in Missile Guidance Theory*, American Institute of Aeronautics and Astronautics, Inc. (1998).
[5]Shneydor, N. A., *Missile Guidance and Pursuit: Kinematics, Dynamics and Control*, Horwood Publishing (1998).
[6]Locke, A. S., *Principles of Guided Missile Design*, D. Van Nostrand Company, Inc. (1955).
[7]Schumacher, C., and Khargonekar, P. P., "Stability Analysis of a Missile Control System with a Dynamic Inversion Controller," *J. Guid. Control Dyn.* **21**(3) (May–Jun 1998).
[8]Etkin, B., *Dynamics of Atmospheric Flight*, Wiley and Sons (1972).
[9]Basar, T., and Bernhard, P., *H-Infinity Optimal Control and Related Minimax Design Problems*, Birkhauser, Boston, MA (1995).
[10]Bryson, A. E., and Ho, Y-C., *Applied Optimal Control*, Hemisphere Publishing Corporation (1975).
[11]Rhee, I., and Speyer, J. L., "A Game Theoretic Approach to a Finite-Time Disturbance Attenuation Problem," *IEEE Trans. Autom. Control* **36**(9), 1021–1032 (Sep 1991).
[12]Cloutier, J. R., D'Souza, N., and Mracek, C. P., "Nonlinear Regulation and Nonlinear H-Infinity Control via the State-Dependent Riccati Equation Technique: Parts 1&2," in *Proc. First Int. Conf. on Nonlinear Problems in Aviation and Aerospace*, pp. 117–141 (9–11 May 1996).
[13]Cloutier, J. R., Mracek, C. P., Ridgely, D. B., and Hammett, K. D., "State Dependent Riccati Equation Techniques: Theory and Applications," ACC Workshop Tutorial #6 (1998).
[14]Lin, C. F., Wang, Q., Speyer, J. L., Evers, J. H., and Cloutier, J. R., "Integrated Estimation, Guidance, and Control System Design Using Game Theoretic Approach," in *Proc. Am. Control Conf.*, pp. 3220–3224 (1992).
[15]Lin, C. F., Ohlmeyer, E., Bibel, J. E., and Malyevac, S., "Optimal Design of Integrated Missile Guidance and Control," *World Aviation Conf.*, AIAA-985519 (Sep 1998).
[16]Menon, P. K., Ohlmeyer, E. J., et al., "Integrated Design of Agile Missile Guidance and Control Systems," *AIAA Missile Sciences Conf.*, Monterey, CA (Nov 1998).
[17]O'Connell, J., *Stability of the Epic Autopilot*, ND-E-MIS-T-2151, RCA (Oct 1982).
[18]Palumbo, N. F., *A Fully Integrated Guidance and Control System for the Highly Responsive Missile Control System: Advanced Technology Demonstration: Preliminary Development and Results*, A1E(96)U-5-196, JHU/APL, Laurel, MD (7 Oct 1996).
[19]Palumbo, N. F., and Casper, S. G., "Integration of a Missile Autopilot, Guidance Filter and Guidance Law," *AIAA/BMDO Technology Conf.* (Jul 2000).
[20]Pearson, J. D., "Approximation Methods in Optimal Control," *J. Electron. Control* **13**, 453–469 (1962).
[21]Hammett, K. D., *Control of Nonlinear Systems via State Feedback State-Dependent Riccati Equation Techniques*, Ph.D. Dissertation, AFIT (Jun 1997).
[22]Rugh, W. J., and Shamma, J. S., "Research on Gain Scheduling," *Automatica* **36**, 1401–1425 (2000).
[23]Franklin, G. F., Powel, J. D., and Workman, M. L., *Digital Control of Dynamic Systems*, Addison-Wesley Publishers (Jun 1990).
[24]Vaughan, D. R., "A Negative Exponential Solution for the Matrix Riccati Equation," *IEEE Trans. Autom. Control* **14**(2), 72–75 (Feb 1969).
[25]Vaughan, D. R., "A Nonrecursive Algebraic Solution for the Discrete Riccati Equation," *IEEE Trans. Autom. Control* **15**(10), 597–599 (Oct 1970).
[26]Reardon, B. E., Palumbo, N. F., and Casper, S. G., "Simulation-Based Performance Optimization of Missile Guidance and Control Algorithms," *AIAA/MDA 2002 Technol. Conf.* (22–25 Aug 2002).
[27]Spall, J. C., "Multivariate Stochastic Approximation Using a Simultaneous Perturbation Gradient Approximation," *IEEE Trans. Autom. Control* **37**(3), 332–341 (Mar 1992).
[28]Spall, J. C., "Implementation of Simultaneous Perturbation Algorithm for Stochastic Optimization," *IEEE Trans. Aerosp. Electron. Sys.* **34**(3), 817–823 (Jul 1998).
[29]Spall, J. C., "An Overview of the Simultaneous Perturbation Method for Efficient Optimization," *Johns Hopkins APL Tech. Dig.* **19**, 482–492 (1998).

THE AUTHORS

NEIL F. PALUMBO is a member of the APL Principal Professional Staff and a section supervisor in the Guidance, Navigation and Control Group of the Air Defense Systems Department. He joined APL in 1993 after having received a Ph.D. in electrical engineering from Temple University, also in 1993. His interests include control and estimation theory, fault-tolerant restructurable control systems, and neuro-fuzzy inference systems. Dr. Palumbo is also a lecturer at the JHU Whiting School of Engineering in the Part-Time Graduate Studies Program. He is a member of the Institute of Electrical and Electronics Engineers and the American Institute of Aeronautics and Astronautics. His e-mail address is neil.palumbo@jhuapl.edu.

BRIAN E. REARDON is a member of the APL Associate Professional Staff in the Air Defense Systems Department. He received B.S. and M.S. degrees in electrical engineering from Drexel University in 2000. Mr. Reardon joined the Guidance, Navigation and Control Group at APL the same year and has been working on missile autopilots, simulation-based performance optimization, and integrated guidance and control. He is a member of the Institute of Electrical and Electronics Engineers. His e-mail address is brian.reardon@jhuapl.edu.

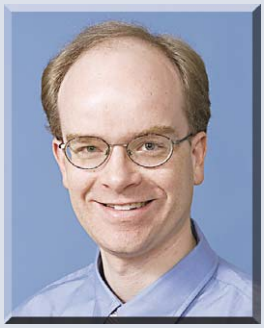

ROSS A. BLAUWKAMP is a member of the APL Senior Professional Staff in the Air Defense Systems Department. He received a B.S.E. degree from Calvin College in 1991 and an M.S.E. degree from the Universty of Illinois in 1996, both in electrical engineering. He continues to pursue a Ph.D. from the University of Illinois. Mr. Blauwkamp joined the Guidance, Navigation and Control Group at APL in 2000. He is currently involved in the design of guidance laws under uncertainty and in the analysis of switching systems for missile control. He is a member of the Institute of Electrical and Electronics Engineers. His e-mail address is ross.blauwkamp@jhuapl.edu.